

# Prototype-Guided Diffusion for Digital Pathology: Achieving Foundation Model Performance with Minimal Clinical Data

Ekaterina Redekop      Mara Pleasure      Vedrana Ivezic      Zichen Wang  
 eredekop@g.ucla.edu      mpleasure@g.ucla.edu      vivezic@g.ucla.edu      zcwang0702@ucla.edu

Kimberly Flores      Anthony Sisk      William Speier  
 KimberlyFlores@mednet.ucla.edu      ASisk@mednet.ucla.edu      Speier@ucla.edu

Corey Arnold  
 cwarnold@ucla.edu

University of California, Los Angeles, USA

## Abstract

*Foundation models in digital pathology use massive datasets to learn useful compact feature representations of complex histology images. However, there is limited transparency into what drives the correlation between dataset size and performance, raising the question of whether simply adding more data to increase performance is always necessary. In this study, we propose a prototype-guided diffusion model to generate high-fidelity synthetic pathology data at scale, enabling large-scale self-supervised learning and reducing reliance on real patient samples while preserving downstream performance. Using guidance from histological prototypes during sampling, our approach ensures biologically and diagnostically meaningful variations in the generated data. We demonstrate that self-supervised features trained on our synthetic dataset achieve competitive performance despite using  $\sim 60x$ – $760x$  less data than models trained on large real-world datasets. Notably, models trained using our synthetic data showed statistically comparable or better performance across multiple evaluation metrics and tasks, even when compared to models trained on orders of magnitude larger datasets. Our hybrid approach, combining synthetic and real data, further enhanced performance, achieving top results in several evaluations. These findings underscore the potential of generative AI to create compelling training data for digital pathology, significantly reducing the reliance on extensive clinical datasets and highlighting the efficiency of our approach.*

## 1. Introduction

Recent advances in deep learning for digital pathology have been powered by large-scale foundation models trained on extensive histopathology datasets with self-supervised learning (SSL). This research has primarily focused on scaling up dataset sizes, driven by the assumption that more data inherently improves performance. One of the first examples, UNI, is a foundation model for pathology, pre-trained using more than 100 million images [7]. Another widely used recent foundational model, Prov-GigaPath, was pre-trained on 1.3 billion pathology images [27]. This trend is further reflected in efforts to expand pathology image repositories based on existing evidence that indicates increasing data volume consistently improves downstream performance [4]. While this notion is intuitive and supported by experimental results, the exact technical reasons for increased performance have been less thoroughly explored, and more importantly, there is little work showing if alternative methods could produce similar results. One alternative to accumulating more data is to use generative modeling to artificially expand training datasets [28, 29, 31]. By utilizing data augmentation to enrich the diversity and quality of pretraining datasets, the downstream performance can be improved. For example, it has been shown that increasing the ratio of synthetic to real data to 100% increases the classifier’s accuracy by up to 6.4% and F1 score by up to 6.6% [1, 31, 38]. In the field of medical imaging, such an approach would be advantageous given the challenges of collecting medical data and ensuring its security and compliant use. Diffusion models, through their iterative noise-and-denoising learning process, have emerged as a powerful tool for dataset augmentation, surpassing the performance of competing generative models such as generative adver-

serial networks (GANs) [12]. Moreover, conditioning a diffusion model’s generation process on various inputs, such as class labels or text, allows for precise control over image creation. This capability to support task-specific augmentation has sparked active research into synthetic data generation for digital pathology [1, 17, 20, 21, 23].

Although diffusion models have shown promise in generating synthetic histopathology images, existing approaches cannot guarantee clinically meaningful diversity in their outputs. Our work addresses this limitation by incorporating structured prior knowledge to produce both diverse and realistic samples. We introduce a prototype-guided diffusion model to generate high-quality synthetic histopathology images, thus ensuring clinically meaningful diversity. Rather than assuming that every real image contains equally valuable information, we use a clustering technique to identify prototypical tissue types. These prototypes distill a large and complex dataset into its essential components, effectively capturing the core concepts needed to describe the underlying pathology. By incorporating these prototypes into training, we ensure that subsequent synthetic data remains both biologically meaningful and diverse. We then pre-train an SSL framework on the generated dataset and evaluate its effectiveness through multiple downstream pathology classification tasks, including subtyping and survival prediction, using an attention-based multiple instance learning (ABMIL) framework [14]. Our results demonstrate that with a relatively tiny amount of real data, our techniques can produce downstream predictive models that have comparable performance to those that require massive amounts of real data. Our methodology may expedite model development by more efficiently utilizing small datasets, ultimately increasing the pace of innovation in the field of digital pathology.

Our contributions are: 1) a novel synthetic data curation method for SSL in digital pathology, using diffusion models guided by histological prototypes derived from clustering; 2) the first digital pathology foundation model trained on 1.7 million synthetically generated images, achieving performance comparable to models trained on clinical datasets that are 60 times larger; 3) a comprehensive evaluation of five subtyping and three survival tasks across various cancer types.

## 2. Related work

### 2.1. Data curation for self-supervised learning

Previous efforts in data curation for SSL have emphasized the importance of constructing datasets that are extensive in size and encompass a diverse range of samples while maintaining a balanced distribution across disease categories [26]. To achieve balanced data subsampling, a popular strategy is to use clustering techniques such as k-means,

where centroids serve as representative points for data subsets. A hierarchical k-means clustering algorithm for automated balanced dataset curation from uncurated data was proposed by Vo et al. [26], yielding substantial downstream performance improvements when self-supervised learning features were trained on the resulting curated datasets.

Van et al. [25] took a different approach and proposed solving a problem of balanced data subset selection as a graph-matching task where the goal is to select the most distinct subset utilizing pairwise similarities. The authors showed substantial downstream performance improvement by training a self-supervised learning algorithm on the re-balanced dataset.

Given the critical role of data diversity and balance in SSL, our work extends these ideas by leveraging histological prototypes to guide the generation of synthetic pathology datasets. Unlike prior efforts that focus solely on selecting subsets from existing data, our approach actively generates new samples to enhance morphological diversity while preserving diagnostic relevance.

### 2.2. Histological prototypes

Tissue prototypes can be identified as clusters of morphologically similar regions within tissue samples [8, 24]. These prototypes are typically represented as centroids derived from clustering, capturing distinctive morphological features present in the tissue. Utilizing tissue prototypes has shown success in recent applications in digital pathology, e.g., prototypical MIL (DeepAttnMISL) [30], which aggregates patch embeddings within the same cluster, followed by aggregating the pooled cluster embeddings. Recently, an unsupervised method that utilizes a Gaussian mixture model to create compact, interpretable representations of whole slide images through morphological prototypes was proposed by Song et al. [24] as an alternative to MIL approaches. Extensive evaluation demonstrated its competitive performance against supervised methods.

Building upon these prior works, our framework integrates histological prototypes into a generative model, ensuring that synthetic pathology images preserve biologically meaningful patterns. Unlike previous methods that use prototypes primarily for feature extraction, we incorporate them directly into the image generation process, creating a synthetic dataset that reflects real-world histological diversity.

### 2.3. Conditional diffusion models for data augmentation

While unconditional diffusion models can generate diverse images without explicit supervision, conditional diffusion models offer greater control over the generated outputs, making them more suitable for clinically meaningful applications [10, 35]. For example, Yellapragada et al. proposed

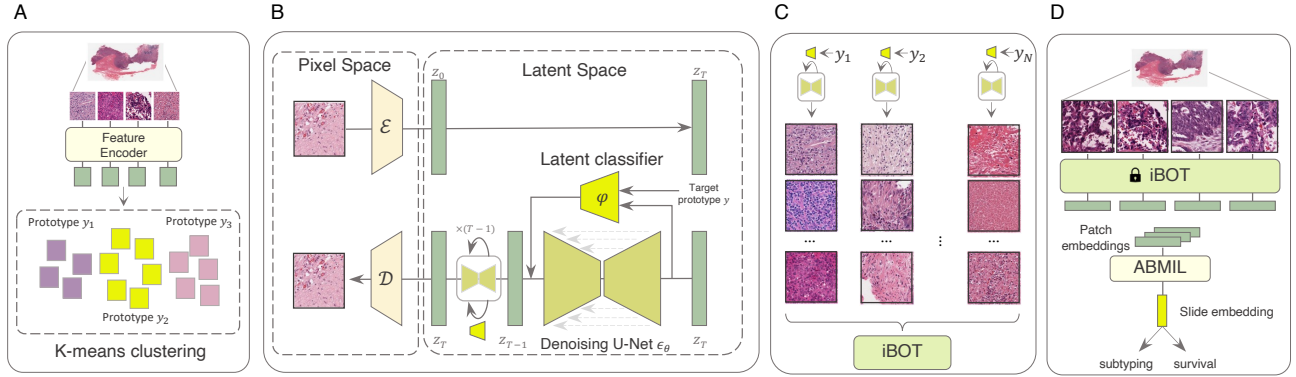


Figure 1. Overview of the proposed approach. **A.** A WSI is segmented and patched into a set of non-overlapping patches. A compressed feature for each patch is obtained through a pre-trained feature encoder. K-Means clustering is performed to identify prototypes within each cancer type. **B.** A latent autoencoder (AE) and a latent diffusion model (LDM) are trained on a large-scale dataset of histopathology images paired with prototype values obtained from clustering for conditional image synthesis under the guidance of a trained latent classifier. **C.** Sampling a fixed number of images from the LDM, guided by each prototype, to construct a synthetic dataset for SSL model training. **D.** We test the proposed method and baselines with few-shot learning on clinical downstream tasks (subtyping and survival prediction).

to use histopathology reports to condition diffusion model training and achieved a SOTA text-to-image generation performance [33].

However, training conditional models requires a large amount of labeled data, which is often difficult to obtain in medical imaging domains. Ye et al. [32] addressed this challenge by introducing a two-stage diffusion-based method for high-quality digital pathology data generation, involving initial unconditional latent diffusion model training on a large unlabeled dataset, followed by fine-tuning on a smaller labeled cohort. The original dataset was augmented with data generated by the proposed method, which led to a significant 6.4% classification improvement in one downstream task.

In this work, we propose an extension of this method by introducing an unsupervised histological prototype-guided approach to generate a comprehensive synthetic dataset that is used to pretrain an SSL model. Unlike the previous method that requires a small labeled subset for conditional generation, our approach uses unsupervised prototypes, enabling controlled data generation without the need for labeled examples. This approach reduces reliance on clinical samples while maintaining strong downstream performance, offering a scalable solution for training robust pathology models with minimal real data.

### 3. Methods

In this study, we propose a prototype-guided diffusion framework for generating synthetic histopathology data, and we demonstrate its utility in SSL and downstream tasks (see Figure 1). We first identify histological prototypes by clustering to find morphologically similar regions within

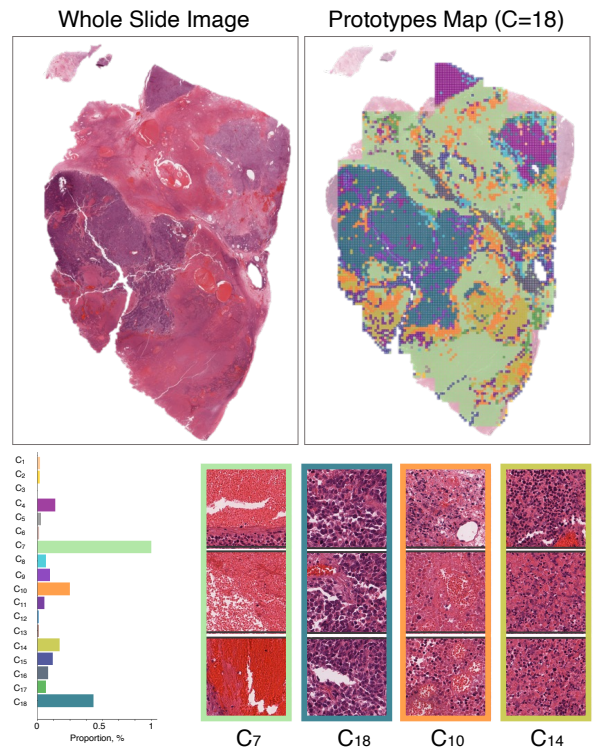


Figure 2. Example of a WSI from TCGA-UCS (Uterine Carcinosarcoma) with its corresponding prototype map, showing 18 detected clusters for this cancer type, along with prototype distribution for the slide and patch examples from the four largest clusters.

tissue samples. Using the extracted prototypes, we then train a conditional latent diffusion model to generate high-

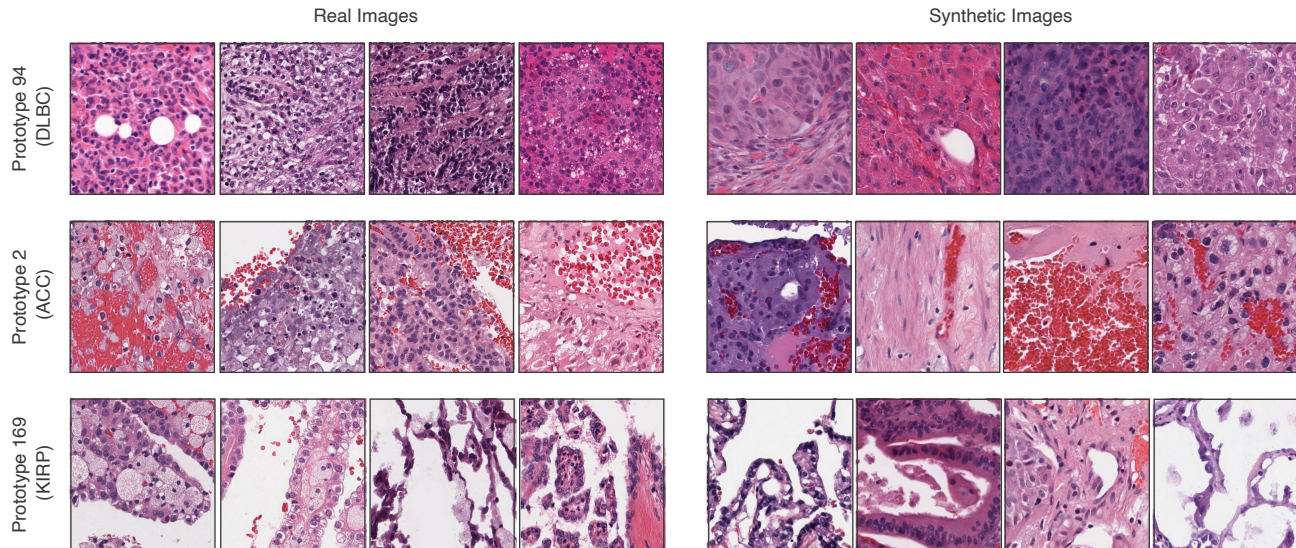


Figure 3. Comparison of real images from the training subset with images generated using prototype guidance for three prototypes, each representing a different tissue type: DLBC (Diffuse Large B-Cell Lymphoma), ACC (Adrenocortical Carcinoma), and KIRP (Kidney Renal Papillary Cell Carcinoma).

fidelity synthetic pathology images. The generated dataset is used to pre-train an SSL framework, learning rich feature representations without requiring labeled pathology data. This framework enables the development of generalizable embeddings that capture essential histological features. Finally, we evaluate the effectiveness of the SSL-pretrained features by training an ABMIL model to aggregate patch-level features and make slide-level predictions.

### 3.1. Histological prototypes

Starting with a collection of WSIs  $X_j, j=1, \dots, J$  from the pretraining cohort  $\mathcal{D}$  spanning  $J$  organs, we extract non-overlapping patches  $X_j = \{x_j^1, \dots, x_j^{N_j}\}$ , where each patch  $x_j^n \in \mathbb{R}^{W \times H \times 3}$ , and transform them into compressed feature embeddings  $\{h_j^1, \dots, h_j^{N_j}\}$  using an encoder pre-trained on  $\mathcal{D}$  [6].

We utilize k-means clustering within each organ-specific subset  $X_j$ . Rather than clustering the entire subset directly, we first draw a uniform sample  $\mathcal{D}'_i \sim \mathcal{D}_i$ , where  $|\mathcal{D}'_i| \ll |\mathcal{D}_i|$  and  $1 \leq i \leq 32$ . This sampling strategy mitigates computational inefficiency while preserving the representative structure of the data. We then apply fine-grained K-means clustering on each sampled subset:

$$S_i \leftarrow \text{K-means}(\mathcal{D}'_i) \quad (1)$$

where the final set of learned cluster centers is given by  $S = \bigcup S_i$ .

To identify the optimal number of clusters within each organ-specific cohort, we calculated the within-cluster sum

of squares (WCSS). Using the "elbow" method, we determined the point at which further increases in the number of clusters led to WCSS diminishing. This approach enabled us to balance capturing meaningful biological variability while preventing unnecessary fragmentation of the data.

### 3.2. Classifier-guided latent diffusion model

We utilize Latent Diffusion Models (LDM) [22], which offer a more computationally efficient alternative to previous approaches [10] while maintaining performance quality. LDM use a two-stage process, beginning with training a latent autoencoder (AE) [15] to compress images into a lower-dimensional latent space. Then, a diffusion model is trained to generate images by learning the distribution of these latent representations.

Specifically, given an image  $x_0 \in \mathbb{R}^{H \times W \times 3}$ , a pre-trained latent autoencoder  $\mathcal{E}$  maps it to a latent representation  $z_0$ :

$$z_0 = E(x_0), \quad z_0 \in \mathbb{R}^{h \times w \times c}, \quad (2)$$

where  $h$ ,  $w$ , and  $c$  are the dimensions of the latent space. The forward diffusion process gradually adds Gaussian noise to  $z_0$  over  $T$  timesteps:

$$q(z_t|z_{t-1}) = \mathcal{N}(z_t; \sqrt{1 - \beta_t}z_{t-1}, \beta_t I), \quad (3)$$

where  $\beta_t$  controls the noise scale at each step. The reverse process learns to reconstruct the latent representation by parameterizing:

$$p_\theta(z_{t-1}|z_t) = \mathcal{N}(z_{t-1}; \mu_\theta(z_t, t), \Sigma_\theta(z_t, t)), \quad (4)$$

where  $\mu_\theta(z_t, t)$  and  $\Sigma_\theta(z_t, t)$  are the predicted mean and covariance.

To introduce classifier guidance, we train a classifier  $C_\phi(y|z_t, t)$  on latent representations, which helps refine the generation process. The mean update in the reverse process is modified as:

$$\tilde{\mu}_\theta(z_t, t, y) = \mu_\theta(z_t, t) + w \cdot \Sigma_\theta(z_t, t) \nabla_{z_t} \log C_\phi(y|z_t, t), \quad (5)$$

where  $w$  is the guidance scale that controls how strongly the classifier influences generation. The reverse diffusion process generates a novel latent  $\tilde{z}_0$  satisfying the class condition  $y$  through a Markov chain that starts from Gaussian noise  $z_T \sim \mathcal{N}(0, I)$ , using the following class-conditioned sampling step:

$$p_{\theta, \phi}(z_{t-1}|z_t, y) = \mathcal{N}(z_{t-1}; \hat{\mu}_\theta(z_t|y), \Sigma_\theta(z_t)). \quad (6)$$

Finally, after sampling a latent  $z_0$ , the decoder  $D$  reconstructs the image:

$$\hat{x}_0 = D(z_0). \quad (7)$$

In our application,  $C_\phi$  is trained to classify histological prototypes, ensuring that the generated synthetic pathology images maintain biologically meaningful variations while enhancing data diversity.

### 3.3. Slide encoding

For a given histology slide, we adopt the ABMIL training paradigm [14, 16], which involves partitioning the slide into smaller patches, extracting feature representations for each patch using a pre-trained vision encoder, and subsequently aggregating these patch-level embeddings to generate a holistic slide-level representation using a trainable attention-based pooling mechanism.

**Pre-trained feature encoder:** We trained from scratch a ViT-Base (86 million parameters) with iBOT [36] on 1.4 million synthetically generated H&E patches sampled uniformly from each tissue prototype. So far, this is the largest SSL model trained solely on synthetically generated data. We denote feature embeddings for slide  $X_i$  as  $H_i \in \mathbb{R}^{N_H \times d_h}$ , where  $N_H$  - number of patches and  $d_h$  - dimensionality of each patch-based feature vector.

**ABMIL slide encoding:** We employ the widely used ABMIL model, which learns patch-specific attention weights to selectively aggregate patch embeddings  $H_i$  into a comprehensive slide representation  $h_i$ .

## 4. Experiments and Results

### 4.1. Datasets

For prototype extraction and LDM training, we utilized FFPE (formalin-fixed, paraffin-embedded) H&E-stained diagnostic slides from 32 cancer types within The Cancer Genome Atlas (TCGA) dataset, leveraging the consistently processed and patched data released as part of the CPIA dataset [34]. The patches were originally 384×384×3, but a center crop was applied to resize them to 224×224×3.

The prototype extraction process yielded a total of 578 prototypes spanning 32 distinct cancer types (see example in Figure 2). We trained two separate versions of iBOT using two distinct datasets. First, a fully synthetic dataset was created by sampling 3,000 patches per prototype using our prototype-guided LDM, resulting in 1,734,000 patches (iBOT-Synth). Second, a combined dataset was formed by augmenting the synthetic data with 3,000 randomly sampled patches per prototype from the TCGA dataset, resulting in 3,468,000 (iBOT-Hybrid).

We compared the performance of iBOT-Synth and iBOT-Hybrid to UNI using five downstream subtyping tasks, two survival, and one prostate cancer biochemical recurrence (BCR) tasks. Our six different subtyping tasks are Non-Small Cell Lung Carcinoma (NSCLC) subtyping on PLCO [37] (two classes), ISUP grading based on Prostate cancer grade assessment (PANDA) challenge [5] (six classes), classification of breast cancer metastases in lymph nodes (Camelyon16) [3, 18] (three classes), ovarian cancer subtypes classification (UBC-OCEAN) challenge [2, 11] (five classes), and PLCO Breast cancer subtyping classification (three classes) [37]. Survival tasks included Breast Invasive Carcinoma (BRCA) and Non-Small Cell Lung Carcinoma (NSCLC) from PLCO. One private dataset from our institution was used for prostate cancer BCR prediction. For all downstream tasks, we performed a patient-level, label-stratified split into training, validation, and test sets with a 70:10:20 ratio unless a predefined split was provided.

### 4.2. Implementation Details

We utilized publicly available implementations and pre-trained weights for all baseline foundation models used for comparison, following the official preprocessing pipelines provided in their respective repositories to maintain consistency with their original training procedures. No further fine-tuning or additional training was applied beyond the publicly released checkpoints.

For the downstream tasks, ABMIL models were trained from scratch using an identical set of hyperparameters across all downstream experiments. We employ a weight decay of  $1 \times 10^{-5}$  and use the AdamW optimizer with a learning rate of  $1 \times 10^{-4}$ , along with a cosine decay scheduler. For the slide classification experiments, we utilized a

	Lung		Prostate		Lymph Nodes		Ovarian		Breast	
	PLCO		PANDA		Camelyon		UBC-OCEAN		PLCO	
	AUC	F1								
UNI	<u>0.971</u>	0.893	<b>0.932</b>	0.668	0.960	0.817	<b>0.978</b>	<b>0.891</b>	<b>0.797</b>	0.550
Prov-GigaPath	0.970	0.901	0.725	0.339	0.930	<b>0.883</b>	0.942	0.759	0.696	0.504
CONCH	0.970	<b>0.913</b>	0.909	0.623	0.818	0.744	0.965	0.829	0.767	0.516
iBOT-Synth	0.967	0.875	0.918	0.648	0.949	0.798	0.962	0.821	0.738	0.525
iBOT-Hybrid	<b>0.974</b>	0.893	<u>0.929</u>	<b>0.673</b>	<b>0.965</b>	0.878	<u>0.972</u>	<u>0.833</u>	<u>0.785</u>	<b>0.583</b>

Table 1. **Subtyping prediction** results of iBOT-Synth (fully synthetic dataset) iBOT-Hybrid (synthetic + TCGA) and baselines for five different subtyping tasks. The best performance is in bold, and the second best is underlined.

cross-entropy loss. We employed early stopping if the validation loss failed to improve over ten consecutive epochs with total training epochs of 20. For survival prediction experiments, we used negative log-likelihood loss (NLL). ABMIL architecture used in the downstream experiments consists of three components. First, a 2-layer MLP with 256 or 512 hidden units, layer normalization, ReLU activation, and 0.25 dropout. This is followed by a gated-attention network consisting of 2-layer MLP, with Sigmoid and Tanh activation, respectively, and 0.25 dropout. Finally, a post-attention linear classification layer with 256 or 512 hidden units is applied.

### 4.3. Results

We used the Fréchet Inception Distance (FID) score [13] to assess the image quality of the synthetic samples, with the achieved value of 0.12 indicating high image quality [32]. Additionally, we qualitatively evaluated the results of the prototype-guided diffusion model used to generate data for iBOT-Synth and iBOT-Hybrid (see Figure 3).

We evaluated our iBOT-Synth and iBOT-Hybrid models against three baseline encoders, noting significant dataset size variations: UNI [7] (100 million images,  $\sim 60\times$  larger than iBOT-Synth), CONCH [19] (1.17 million image-caption pairs, comparable to iBOT-Synth), and Prov-GigaPath [27] (1.3 billion images,  $\sim 760\times$  larger than iBOT-Synth). Features extracted from these encoders were used within an ABMIL framework trained to perform cancer subtyping and survival prediction. To assess the statistical significance between subtyping models, we perform a Wilcoxon Signed-Rank Test to evaluate the observed differences in performance between the two models [27]. To statistically compare the survival models, we use DeLong’s test to compare the concordance index (c-index) [9].

#### 4.3.1. Cancer Subtyping

Both iBOT-Synth and iBOT-Hybrid models show competitive performance across all cancer types in both AUROC and F1-score metrics (see Table 1). Notably, iBOT-Hybrid trained on  $\sim 30$  times fewer data points than UNI and  $\sim 380$  times fewer data points than Prov-GigaPath outperforms

both models in AUC in lung and lymph node cancer subtyping tasks and shows the second highest AUC among all other cancer types. iBOT-Hybrid results in the highest F1 for prostate and breast subtyping tasks and shows the second highest F1 for lymph nodes and ovarian tasks. Compared to UNI, iBOT-Hybrid demonstrates significantly better performance in the lung ( $p=0.016$ ) and lymph nodes ( $p<0.01$ ) cancer subtyping tasks. Additionally, there is no significant difference between iBOT-Hybrid and UNI for the ovarian ( $p=0.14$ ) cancer subtyping task. Statistical testing shows no significant difference between iBOT-Hybrid and CONCH for lung ( $p=0.11$ ) and ovarian ( $p=0.053$ ) cancer subtyping tasks. iBOT-Hybrid significantly outperforms CONCH for prostate ( $p<0.01$ ), lymph nodes ( $p<0.01$ ), and breast ( $p<0.01$ ) cancer subtyping tasks. Compared to Prov-GigaPath, iBOT-Hybrid demonstrated no significant performance difference in the lung cancer subtyping task ( $p=0.24$ ) but achieved significantly better results in all other subtyping tasks.

Statistical significance testing confirmed that while iBOT-Synth, trained entirely on synthetic data, was slightly outperformed by iBOT-Hybrid, it still achieved competitive performance. Notably, UNI was trained on  $\sim 60$  times more data, while Prov-GigaPath utilized  $\sim 760$  times more data. CONCH, trained on approximately the same amount of data, incorporated an additional modality, introducing an extra challenge compared to iBOT-Synth. Despite these significant differences in training data, there was no statistically significant difference between the prediction of iBOT-Synth and UNI on three out of five cancer subtyping tasks: lung ( $p=0.25$ ), prostate ( $p=0.36$ ), and ovarian ( $p=0.22$ ). iBOT-Synth showed no significant difference in performance compared to CONCH for three out of five cancer subtyping tasks: lung ( $p=0.77$ ), breast ( $p=0.23$ ), and ovarian ( $p=0.21$ ). iBOT-Synth did show significantly different performance than CONCH on the prostate ( $p<0.01$ ) and lymph nodes ( $p<0.01$ ) tasks. Compared to Prov-GigaPath, iBOT-Synth demonstrated no significant performance difference in the lung cancer subtyping task ( $p=0.58$ ) but achieved significantly better results in prostate classification ( $p<0.01$ ), lymph nodes ( $p<0.01$ ), ovarian ( $p<0.01$ ),

and breast ( $p < 0.01$ ) cancer subtyping tasks.

	Lung	Prostate BCR	Breast
	PLCO	Private	PLCO
	c-index	c-index	c-index
UNI	<u>0.578</u>	0.632	0.560
Prov-GigaPath	0.595	0.664	0.560
CONCH	0.544	0.603	0.555
iBOT-Synth	0.572	<u>0.7</u>	<b>0.585</b>
iBOT-Hybrid	<b>0.636</b>	<b>0.704</b>	<u>0.580</u>

Table 2. **Survival and prostate BCR prediction** results of iBOT-Synth (fully synthetic dataset) iBOT-Hybrid (synthetic + TCGA) and baselines for two survival and one prostate BCR task. The best performance is in bold, and the second best is underlined.

### 4.3.2. Survival Prediction and Prostate BCR Analysis

We used the c-index for survival and prostate cancer BCR evaluation (see Table 2). In lung cancer survival prediction, iBOT-Hybrid achieves the highest c-index of 0.636, indicating the highest performance among all models. Prov-GigaPath also demonstrates strong performance with a c-index of 0.595, while UNI achieves 0.578. iBOT-Synth shows a competitive result of 0.572, suggesting that even with fully synthetic data, it maintains reasonable predictive power. CONCH, however, shows significantly lower performance in this task. iBOT-Hybrid significantly outperformed UNI ( $p < 0.01$ ), Prov-GigaPath ( $p < 0.01$ ) and CONCH ( $p < 0.01$ ). iBOT-Synth significantly outperformed CONCH ( $p < 0.01$ ) but showed no significant difference when compared to UNI ( $p = 0.12$ ) and Prov-GigaPath ( $p = 0.32$ ).

For prostate BCR prediction, both iBOT-Synth and iBOT-Hybrid achieve the highest c-index values, with 0.70 and 0.704, respectively. This indicates that our models are particularly effective in predicting prostate BCR, demonstrating statistically significant improvements over the three baseline methods. Prov-GigaPath shows a c-index of 0.664, while UNI achieves 0.632. CONCH again shows lower performance.

In breast cancer survival prediction, iBOT-Synth achieves the highest c-index of 0.585. iBOT-Hybrid also performs well with a c-index of 0.580. UNI and Prov-GigaPath both achieve 0.560, while CONCH shows 0.555. iBOT-Hybrid didn't show a statistically significant difference with UNI ( $p = 0.055$ ) and Prov-GigaPath ( $p = 0.061$ ), but significantly outperformed CONCH ( $p < 0.01$ ). iBOT-Synth significantly outperformed UNI ( $p < 0.01$ ), Prov-GigaPath ( $p < 0.01$ ) and CONCH ( $p < 0.01$ ).

## 5. Conclusions

In conclusion, this study explores the potential of a prototype-guided diffusion model to generate high-fidelity

synthetic pathology data, reducing the need for large, real-world datasets in digital pathology. Our approach enables large-scale self-supervised learning while ensuring biologically meaningful variations in the generated data. We demonstrate that self-supervised features trained on our synthetic dataset achieve competitive performance, using up to 760 times less data than models trained on large real-world datasets. Notably, our models showed statistically comparable or superior performance across various evaluation metrics. Additionally, combining synthetic and real data further enhanced performance, achieving top results in several downstream tasks. These findings highlight the effectiveness of generative AI in reducing reliance on extensive clinical datasets, offering a more efficient approach for training models in digital pathology.

## References

- [1] Panagiotis Alimisis, Ioannis Mademlis, Panagiotis Radoglou-Grammatikis, Panagiotis Sarigiannidis, and Georgios Th Papadopoulos. Advances in diffusion models for image data augmentation: A review of methods, models, evaluation metrics and future research directions. *Artificial Intelligence Review*, 58(4):1–55, 2025. 1, 2
- [2] Maryam Asadi-Aghbolaghi, Hossein Farahani, Allen Zhang, Ardalan Akbari, Sirim Kim, Ashley Chow, Sohier Dane, OCEAN Challenge Consortium, OTTA Consortium, David G Huntsman, et al. Machine learning-driven histotype diagnosis of ovarian carcinoma: Insights from the ocean ai challenge. *medRxiv*, pages 2024–04, 2024. 5
- [3] Babak Ehteshami Bejnordi, Mitko Veta, Paul Johannes Van Diest, Bram Van Ginneken, Nico Karssemeijer, Geert Litjens, Jeroen AWM Van Der Laak, Meyke Hermesen, Quirine F Manson, Maschenka Balkenhol, et al. Diagnostic assessment of deep learning algorithms for detection of lymph node metastases in women with breast cancer. *Jama*, 318(22):2199–2210, 2017. 5
- [4] Mohsin Bilal, Manahil Raza, Youssef Altherwy, Anas Al-suhaibani, Abdulrahman Abduljabbar, Fahdah Almarshad, Paul Golding, Nasir Rajpoot, et al. Foundation models in computational pathology: A review of challenges, opportunities, and impact. *arXiv preprint arXiv:2502.08333*, 2025. 1
- [5] Wouter Bulten, Kimmo Kartasalo, Po-Hsuan Cameron Chen, Peter Ström, Hans Pinckaers, Kunal Nagpal, Yuannan Cai, David F Steiner, Hester Van Boven, Robert Vink, et al. Artificial intelligence for diagnosis and gleason grading of prostate cancer: the panda challenge. *Nature medicine*, 28(1):154–163, 2022. 5
- [6] Richard J Chen, Chengkuan Chen, Yicong Li, Tiffany Y Chen, Andrew D Trister, Rahul G Krishnan, and Faisal Mahmood. Scaling vision transformers to gigapixel images via hierarchical self-supervised learning. In *Proceedings of the IEEE/CVF conference on computer vision and pattern recognition*, pages 16144–16155, 2022. 4
- [7] Richard J Chen, Tong Ding, Ming Y Lu, Drew FK Williamson, Guillaume Jaume, Andrew H Song, Bowen

- Chen, Andrew Zhang, Daniel Shao, Muhammad Shaban, et al. Towards a general-purpose foundation model for computational pathology. *Nature Medicine*, 30(3):850–862, 2024. 1, 6
- [8] Adalberto Claudio Quiros, Nicolas Coudray, Anna Yeaton, Xinyu Yang, Bojing Liu, Hortense Le, Luis Chiriboga, Afreen Karimkhan, Navneet Narula, David A Moore, et al. Mapping the landscape of histomorphological cancer phenotypes using self-supervised learning on unannotated pathology slides. *Nature Communications*, 15(1):4596, 2024. 2
- [9] Elizabeth R DeLong, David M DeLong, and Daniel L Clarke-Pearson. Comparing the areas under two or more correlated receiver operating characteristic curves: a nonparametric approach. *Biometrics*, pages 837–845, 1988. 6
- [10] Prafulla Dhariwal and Alexander Nichol. Diffusion models beat gans on image synthesis. *Advances in neural information processing systems*, 34:8780–8794, 2021. 2, 4
- [11] Hossein Farahani, Jeffrey Boschman, David Farnell, Amirali Darbandsari, Allen Zhang, Pouya Ahmadvand, Steven JM Jones, David Huntsman, Martin Köbel, C Blake Gilks, et al. Deep learning-based histotype diagnosis of ovarian carcinoma whole-slide pathology images. *Modern Pathology*, 35(12):1983–1990, 2022. 5
- [12] Ian Goodfellow, Jean Pouget-Abadie, Mehdi Mirza, Bing Xu, David Warde-Farley, Sherjil Ozair, Aaron Courville, and Yoshua Bengio. Generative adversarial networks. *Communications of the ACM*, 63(11):139–144, 2020. 2
- [13] Martin Heusel, Hubert Ramsauer, Thomas Unterthiner, Bernhard Nessler, and Sepp Hochreiter. Gans trained by a two time-scale update rule converge to a local nash equilibrium. *Advances in neural information processing systems*, 30, 2017. 6
- [14] Maximilian Ilse, Jakub Tomczak, and Max Welling. Attention-based deep multiple instance learning. In *International conference on machine learning*, pages 2127–2136. PMLR, 2018. 2, 5
- [15] Diederik P Kingma, Max Welling, et al. Auto-encoding variational bayes, 2013. 4
- [16] Jiayun Li, Wenyuan Li, Anthony Sisk, Huihui Ye, W Dean Wallace, William Speier, and Corey W Arnold. A multi-resolution model for histopathology image classification and localization with multiple instance learning. *Computers in biology and medicine*, 131:104253, 2021. 5
- [17] Jasper Linmans, Gabriel Raya, Jeroen van der Laak, and Geert Litjens. Diffusion models for out-of-distribution detection in digital pathology. *Medical Image Analysis*, 93: 103088, 2024. 2
- [18] Geert Litjens, Peter Bandi, Babak Ehteshami Bejnordi, Oscar Geessink, Maschenka Balkenhol, Peter Bult, Altuna Halilovic, Meyke Hermsen, Rob Van de Loo, Rob Vogels, et al. 1399 h&e-stained sentinel lymph node sections of breast cancer patients: the camelyon dataset. *GigaScience*, 7(6):giy065, 2018. 5
- [19] Ming Y Lu, Bowen Chen, Drew FK Williamson, Richard J Chen, Ivy Liang, Tong Ding, Guillaume Jaume, Igor Odintsov, Long Phi Le, Georg Gerber, et al. A visual-language foundation model for computational pathology. *Nature Medicine*, 30(3):863–874, 2024. 6
- [20] Matteo Pozzi, Shahryar Noei, Erich Robbi, Luca Cima, Monica Moroni, Enrico Munari, Evelin Torresani, and Giuseppe Jurman. Generating synthetic data in digital pathology through diffusion models: a multifaceted approach to evaluation. *medRxiv*, pages 2023–11, 2023. 2
- [21] Matteo Pozzi, Shahryar Noei, Erich Robbi, Luca Cima, Monica Moroni, Enrico Munari, Evelin Torresani, and Giuseppe Jurman. Generating and evaluating synthetic data in digital pathology through diffusion models. *Scientific Reports*, 14(1):28435, 2024. 2
- [22] Robin Rombach, Andreas Blattmann, Dominik Lorenz, Patrick Esser, and Björn Ommer. High-resolution image synthesis with latent diffusion models. In *Proceedings of the IEEE/CVF conference on computer vision and pattern recognition*, pages 10684–10695, 2022. 4
- [23] Mariia Sidulova, Seyed Kahaki, Ian Hagemann, and Alexej Gossman. Contextual unsupervised deep clustering in digital pathology. In *Conference on Health, Inference, and Learning*, pages 558–565. PMLR, 2024. 2
- [24] Andrew H Song, Richard J Chen, Tong Ding, Drew FK Williamson, Guillaume Jaume, and Faisal Mahmood. Morphological prototyping for unsupervised slide representation learning in computational pathology. In *Proceedings of the IEEE/CVF Conference on Computer Vision and Pattern Recognition*, pages 11566–11578, 2024. 2
- [25] Hugues Van Assel and Randall Balestriero. A graph matching approach to balanced data sub-sampling for self-supervised learning. In *NeurIPS 2024 Workshop: Self-Supervised Learning-Theory and Practice*. 2
- [26] Huy V Vo, Vasil Khalidov, Timothée Darcet, Théo Moutakanni, Nikita Smetanin, Marc Szafraniec, Hugo Touvron, Camille Couprie, Maxime Oquab, Armand Joulin, et al. Automatic data curation for self-supervised learning: A clustering-based approach. *arXiv preprint arXiv:2405.15613*, 2024. 2
- [27] Hanwen Xu, Naoto Usuyama, Jaspreet Bagga, Sheng Zhang, Rajesh Rao, Tristan Naumann, Cliff Wong, Zelalem Gero, Javier González, Yu Gu, et al. A whole-slide foundation model for digital pathology from real-world data. *Nature*, 630(8015):181–188, 2024. 1, 6
- [28] Yuan Xue, Qianying Zhou, Jiarong Ye, L Rodney Long, Sameer Antani, Carl Cornwell, Zhiyun Xue, and Xiaolei Huang. Synthetic augmentation and feature-based filtering for improved cervical histopathology image classification. In *Medical Image Computing and Computer Assisted Intervention–MICCAI 2019: 22nd International Conference, Shenzhen, China, October 13–17, 2019, Proceedings, Part I 22*, pages 387–396. Springer, 2019. 1
- [29] Yuan Xue, Jiarong Ye, Qianying Zhou, L Rodney Long, Sameer Antani, Zhiyun Xue, Carl Cornwell, Richard Zaino, Keith C Cheng, and Xiaolei Huang. Selective synthetic augmentation with histogan for improved histopathology image classification. *Medical image analysis*, 67:101816, 2021. 1
- [30] Jiawen Yao, Xinliang Zhu, Jitendra Jonnagaddala, Nicholas Hawkins, and Junzhou Huang. Whole slide images based cancer survival prediction using attention guided deep multiple instance learning networks. *Medical image analysis*, 65: 101789, 2020. 2

- [31] Jiarong Ye, Yuan Xue, L Rodney Long, Sameer Antani, Zhiyun Xue, Keith C Cheng, and Xiaolei Huang. Synthetic sample selection via reinforcement learning. In *Medical Image Computing and Computer Assisted Intervention–MICCAI 2020: 23rd International Conference, Lima, Peru, October 4–8, 2020, Proceedings, Part I 23*, pages 53–63. Springer, 2020. [1](#)
- [32] Jiarong Ye, Haomiao Ni, Peng Jin, Sharon X Huang, and Yuan Xue. Synthetic augmentation with large-scale unconditional pre-training. In *International Conference on Medical Image Computing and Computer-Assisted Intervention*, pages 754–764. Springer, 2023. [3](#), [6](#)
- [33] Srikar Yellapragada, Alexandros Graikos, Prateek Prasanna, Tahsin Kurc, Joel Saltz, and Dimitris Samaras. Pathldm: Text conditioned latent diffusion model for histopathology. In *Proceedings of the IEEE/CVF Winter Conference on Applications of Computer Vision*, pages 5182–5191, 2024. [3](#)
- [34] Nan Ying, Yanli Lei, Tianyi Zhang, Shangqing Lyu, Chunhui Li, Sicheng Chen, Zeyu Liu, Yu Zhao, and Guanglei Zhang. Cpia dataset: A comprehensive pathological image analysis dataset for self-supervised learning pre-training. *arXiv preprint arXiv:2310.17902*, 2023. [5](#)
- [35] Zheyuan Zhan, Defang Chen, Jian-Ping Mei, Zhenghe Zhao, Jiawei Chen, Chun Chen, Siwei Lyu, and Can Wang. Conditional image synthesis with diffusion models: A survey. *arXiv preprint arXiv:2409.19365*, 2024. [2](#)
- [36] Jinghao Zhou, Chen Wei, Huiyu Wang, Wei Shen, Cihang Xie, Alan Yuille, and Tao Kong. ibot: Image bert pre-training with online tokenizer. *arXiv preprint arXiv:2111.07832*, 2021. [5](#)
- [37] Claire S Zhu, Paul F Pinsky, Barnett S Kramer, Philip C Prorok, Mark P Purdue, Christine D Berg, and John K Gohagan. The prostate, lung, colorectal, and ovarian cancer screening trial and its associated research resource. *Journal of the National Cancer Institute*, 105(22):1684–1693, 2013. [5](#)
- [38] Jingyuan Zhu, Huimin Ma, Jiansheng Chen, and Jian Yuan. Domainstudio: Fine-tuning diffusion models for domain-driven image generation using limited data. 2023. [1](#)